Soft Matter

Accepted Manuscript

ROYAL SOCIETY OF CHEMISTRY

www.rsc.org/softmatter

Soft Matter

ARTICLE

Pressure Sensitive Microparticle Adhesion through Biomimicry of the Pollen-Stigma Interaction

Received 00th January 20xx,
Accepted 00th January 20xx

DOI: 10.1039/x0xx00000x

www.rsc.org/

Haisheng Lin [a], Zihao Qu [a] and J. Carson Meredith [a]

Many soft biomimetic synthetic adhesives, optimized to support macroscopic masses (~ kg), have been inspired by geckos, insects and other animals. Far less work has investigated bioinspired adhesion that is tuned to micro- and nano-scale sizes and forces. However, such adhesive forces are extremely important in the adhesion of micro- and nanoparticles to surfaces, relevant to a wide range of industrial and biological systems. Pollens, whose adhesion is critical to plant reproduction, are an evolutionary-optimized system for biomimicry to engineer tunable adhesion between particles and micro-patterned soft matter surfaces. In addition, the adhesion of pollen particles is relevant to topics as varied as pollinator ecology, transport of allergens, and atmospheric phenomena. We report the first observation of structurally-derived pressure-sensitive adhesion of a microparticle by using the sunflower pollen and stigma surfaces as a model. This strong, pressure-sensitive adhesion results from interlocking between the pollen's conical spines and the stigma's receptive papillae. Inspired by this behavior, we fabricated synthetic polymeric patterned surfaces that mimic the stigma surface's receptivity to pollen. These soft mimics allow the magnitude of the pressure-sensitive response to be tuned by adjusting the size and spacing of surface features. These results provide an important new insight for soft material adhesion based on bio-inspired principles, namely that ornamented microparticles and micro-patterned surfaces can be designed with complementarity that enable a tunable, pressure-sensitive adhesion on the microparticle size and length scale.

Introduction

Efforts to investigate and design novel biomimetic synthetic adhesives inspired by Nature have garnered widespread scientific interest.[1-10] Recent studies on biomimetic adhesive structures have attributed the remarkable adhesion ability of a number of biological systems to microscale and nanoscale hierarchical hairy or fibrillar interfacial structures, including geckos, insect wings and plant leaves.[8-15] Generally, the fascinating adhesion features of those biomimetic structures result from large contact areas generated by the contact of millions of these hierarchical structures via weak but universal van der Waals forces (VDW) and/or collective mechanical interlocking forces.[16-18] In all of these examples, however, the adhesion produced is at a magnitude that is appropriate for macroscopic-sized objects, e.g., 1−10 N/cm^2.[16-18]

In addition, Nature also provides remarkable examples of evolutionary-optimized microscale biological particles with hierarchical structures and/or chemistries tailored for effective adhesion to a variety of natural surfaces. One of the most important examples of these particles is pollen, which must possess features that allow adhesion to be finely tuned on a much smaller scale than those of animals and macroscopic plant surfaces. Pollen particles, possessing a range of ornamentations that vary in morphology (i.e. reticular, echinate) and feature size (10 nm−5 μm), can disperse in air or adhere on insects or other animals, allowing for their distribution over large areas. Flower stigma surfaces typically consist of pattered micron-sized papillae with roughnesses ranging from 200 to 600 nm,[19-21] and pollen adhesion to these receptive papillae on the stigma is a key step in plant reproduction.[22-24] Pollen adhesion is also critical to the complex steps in pollen transport. For example, the pollens of plants pollenated by animals must (i) be easily removed from one flower by the pollinator, (ii) adhere well to the pollinator during transport, and (iii) readily release onto a complementary plant stigma surface. How pollen and stigma surfaces accomplish such feats is not well understood. However, previous studies have established a number of facts that lead us to believe this is a fruitful system for the study of patterns in driving complementary adhesion in soft matter: (i) pollen-stigma interfaces differ from species to species, exhibiting wide variation in morphology; (ii) initial adhesion of pollen on stigmas is generally driven by generic van der Waals interactions; and (iii) stigmas adhere poorly to pollen grains from other botanical families.[22-26] These features suggest that pollen and stigma may demonstrate physical specificity through pattern interlocking.[23]

Our previous studies on pollen adhesion have utilized synthetic flat and relatively smooth substrates that do not mimic the natural patterned surfaces with which pollen interacts.[16-18] Discovery of the existence of such features and the mechanisms by which they function would advance fundamental understanding of soft matter interactions in patterned natural systems and provide inspiration for the biomimicry of these surfaces. For example, several recent

[a] School of Chemical & Biomolecular Engineering, Georgia Institute of Technology, 311 Ferst Drive NW, Atlanta, Georgia 30332-0100. Email: carson.meredith@chbe.gatech.edu;Tel: 1-404-385-2151; Fax: 1-404-894-2866.
Electronic Supplementary Information (ESI) available: [details of any supplementary information available should be included here]. See DOI: 10.1039/x0xx00000x

examples of designed biomimetic patterned surfaces exhibited inspired enhanced complementarity adhesions.[17, 27-32] In the design of new microparticle interfaces, mimicking pollen adhesive mechanisms may enable microscale particles with tailored adhesion for use in drug and agrochemical delivery,[33-36] paints and coatings,[37] and polymer composites.[38] Pollens also provide a unique template from which inorganic metal and metal-oxide particles with unique functionalities (e.g., magnetism) have been produced.[39, 40] Besides the obvious significance to plant biology, these advances may also provide insights to epidemiology of asthma and allergies by understanding how such particles distribute on indoor surfaces.

By using pollen and stigma as a model, we report the first observation of pressure-dependent adhesion of a single microparticle mediated by complementary physical structures. This load-sensitive particle adhesion is mediated by the interlocking patterns on the surfaces of pollen and stigma from the same botanical family. Inspired by this result, we fabricated a series of patterned stigma-mimicking surfaces by using the phase-separation of blends of polystyrene (PS) with a triblock copolymer: polystyrene-*b*-polyisoprene-*b*-polystyrene (PSI). This blend allows facile tuning of the size of the patterns and surface roughness. The stigma mimics displayed load-dependent adhesion with echinate (spiny sunflower and ragweed) pollens that could be adjusted by tuning the size of the mimicked features. In contrast, non-echinate olive pollen from a different botanical family showed no pressure-dependent adhesion on the stigma-mimicking surfaces. These results corresponded well with centrifuge measurements of pollen detachment forces from the biomimetic surfaces. The results provide new insight into both natural pollen adhesion and the engineering of complementary ornamented particles and patterned surfaces to achieve pressure-sensitive adhesion capability of single microparticles that operates on the nN and μm forces and length scales.

Experimental Section

Stigma and Pollen. Clean stigmas of sunflower (*Helianthus annuus*) that lack a copious surface secretion[19] were chosen, shown in Figure 1.Native non-defatted pollen particles were purchased from Greer Laboratories (Lenoir, NC), stored at 0 ºC, and used as received. Pollen particles from three species representing two morphologies were explored, and are shown in Figure 2: olive (*Olea europaea*, Po) from the *Oleaceae* family possessing a nanoscale reticulate (grooved) structure and two echinate (spiked) pollens from the *Asteraceae* family, ragweed (*Ambrosia artemisiifolia*, Pr) and sunflower (*Helianthus annuus*, Psf).The characteristics of all three pollen samples are listed in Table 1. Olive and ragweed are widespread *anemophilous* plants and are coated by only a thin layer of liquid pollenkitt. In contrast, the pollen grains of sunflower (*entomophilous*) are covered by a thick pollenkitt layer,[41, 42]which can be seen to fill cavities and pores in the exine as well as form droplets on the ends of some spines in Figure S1.

The pollenkitt contents of the pollen samples were 8 % by mass (olive), 15 % (ragweed), and 30 % (sunflower).[43]To compare native (_N) pollen carrying pollenkitt (Psf_N, Po_N, Pr_N) to clean pollen (_C) without pollenkitt (Psf_C, Po_C, Pr_C), we applied a solvent washing procedure to remove the pollenkitt. Native pollen samples were washed in a mixture of chloroform and methanol (3:1),[44] for 24 h before being deposited on filter paper (P5, Fisher Scientific, Pittsburgh, PA) supported on a stainless steel 47 mm screen (Kontes Glass, Vineland, NJ). The pollen samples were dried at 40 ºC for at least 12 hours before use. The radii of the pollen morphological features were not changed significantly after the solvent extraction with chloroform/methanol (3:1).The surface chemistry of these three clean pollen particles was almost identical as confirmed by FTIR spectra (Figure S2).

Force Measurements. Adhesion force (F_{ad}) was measured using atomic force microscopy (AFM, Veeco Dimension 3100). Tipless rectangular cantilevers with nominal spring constants of 0.1−0.6 N/m (Applied Nano Structures, Inc., Santa Clara, CA) were used. Single pollen particles were glued to the tipless cantilevers with a small amount of epoxy, as described in detail elsewhere.[45] The real spring constants for the cantilevers with the attached pollen grains were determined by the thermal tune method incorporated in the AFM program. A series of 20 force-distance curves were measured for each pollen-surface combination, taken within the randomly-chosen areas on three substrate surfaces 4 cm × 4 cm at 20 ºC and humidity of 30−35%. The adhesion forces were measured at the final detachment event during retraction of probes from the substrate surfaces. Three separate pollen AFM tips were used for each species. The typical load forces (F_L) during force measurements were 2.5−500 nN, and the scan velocity was 1.0 μm/s.

The cantilevers with pollen particles attached are shown in Figure S1, taken after all force measurements were completed. It is noteworthy that no obvious damage to pollen particles was observed under applied load forces up to 500 nN. Figure S1d−f shows high magnification SEM images for surface ornamentations of each native pollen (with pollenkitt). The pollen particles are not subjected to measureable deformation and do not exhibit compliance under any of the loading forces used here.[45]

Scanning Electron Microscopy (SEM).The sunflower stigma surface and the pollen AFM probes were characterized by scanning electron microscopy (SEM) (LEO 1530 FEG) after all force measurements were finished, at an accelerating potential of 10.0 kV. Probe tips were sputtered with gold and then mounted on metal stubs using carbon tapes.

Fabrication of Stigma Mimicking Patterned Polymer Surfaces. Polystyrene with three different molecular masses (PS1, M_w = 1.3 kDal with M_w/M_n = 1.06; PS2, M_w = 13 kDal with M_w/M_n = 1.06; PS3, M_w = 230 kDal with M_w/M_n = 1.64; Sigma-Aldrich) and polystyrene-block-polyisoprene-block-polystyrene (PSI, 17 % by mass styrene, M_n = 1.9 kDal, Sigma-Aldrich) were used as received. To generate conical-patterned surfaces with PS1, PS2 and PS3 blended with PSI, the mass ratio of PS:PSI was kept at 1:4, and the roughness of the phase-separated pattern was varied by adjusting the PS chain length. Pure PS3 was used as a control smooth surface, hereafter referred to simply as PS. The PS and the blend solutions were prepared by dissolving 10% by mass of the following polymers in toluene: PS = 10% PS3; PSI1 = 2% PS1 + 8% PSI; PSI2 = 2% PS2 + 8% PSI; PSI3 = 2% PS3 + 8% PSI. Polymeric test surfaces were prepared as thin polymer films on Piranha-etched (30/70 vol% H_2O_2/concentrated H_2SO_4 at 80 ºC for 2 h) silicon substrates, by

using a doctor-blade coater. Cast films were dried at room temperature for 24 h and then annealed at 80 ºC under vacuum for 2 h. For reference, the glass transition temperatures of the materials are reported to be T_g= -40 °C (PSI), 30-38 °C (PS1), 90-93 °C (PS2) and 100-104 °C (PS3).[46, 47] Film thickness, measured with an interferometer, was approximately 10 μm, which far exceeds the range of van der Waals interactions (~20 nm) and negates energetic effects of the underlying silicon substrate on the polymer-pollen interactions. As a hydrophilic, flat control surface, piranha-treated Si was utilized in some measurements. The mean (R_a) and root-mean-square (*rms*) surface roughness of each surface (Table 2) were obtained from topography scans of three randomly-chosen 10 μm×10 μm areas on each substrate surface by using AFM.

Detachment Force Measurement. The detachment forces of pollen particles on the patterned mimic polymer surfaces were measured by using a modified centrifuge method. This technique samples a larger number of particles and particle orientations than is feasible with AFM.[48, 49]Pollen particles were deposited freely in air manually on test surfaces (4 cm × 4 cm) that were secured onto glass slides sealed in a slide mailer (VWR®) prior to placing them in the centrifuge. The use of the slide mailer to seal the samples removes drag and frictional forces, thus the detachment forces are due to centrifugal force only. Detachment measurements were performed using a Centra cl2 centrifuge (Thermo Scientific IEC) at various speeds up to 3.5 ×1000 rpm. The distance between the test surface and the axis of rotation was 10 cm. The number of retained pollens was measured successively after 10 min of spinning at rotor speeds of 1.0, 1.5, 2.0, 2.5, 3.0 and 3.5 ×1000 rpm. The relative centrifugal force (RCF, in units of times gravity, × g) was obtained by

$$RCF = 1.118 \times 10^{-5} \times d \times S^2 \quad (1)$$

where d is the rotor radius (cm), and S is centrifuge speed (rpm). The estimated average mass of a single pollen grain is 100 ng.[43, 50, 51] Therefore, the centrifugal force (as the product of a single pollen grain mass and RCF) ranged from 112to 1370nN. All sample handling and centrifugal testing were performed at 20 ºC and humidity 30%.

Results are presented as the retained percentage, r, defined by the ratio of the number of non-detached pollen grains on the surface at centrifuge rotor speed i × 1000 rpm ($r(i)$) to the initial number of pollen grains remaining deposited on the surface at low centrifuge rotor speed (<100 rpm), $r(0)$. A low speed of 100 rpm was used as a reference to gently remove unattached grains and large multi-grain aggregations, so that measurements were based on adhered single pollens. Generally, the value of $r(0)$ fell in the range of 100 to 1000 within each ~15 × 15 mm image area. Results from three images were averaged from each sample. Owing to the variations in pollen orientation, surface roughness, and experimental conditions, the pollen particles detach over a range of centrifugal forces. Thus, in order to represent the overall detachment behavior, the interaction of free pollen particles with surfaces was characterized as the detachment force (F_d), which was defined as the centrifugal force at 50% retained percentage.[52, 53]

Results and Discussion

Pollen-Stigma Interaction

Figure 1 shows photographs of the sunflower and SEM images of its clean stigma surfaces, which display multiple rows of dense micro-conical papillae of approximately 2 μm tip radius, 10 μm height, and spacing of ~2−5 μm (red arrow) in the center of each stigma arm; and long large terminal hairs of ~100−200 μm length (black arrow) at the two outer-edges. When free pollen particles attach to the stigma surface (Figure 1c), multiple spines of pollen interact with stigma papillae. Figure 2 shows the SEM images of clean pollen particles of three different species with varied fine micro-spine exines. For example, the exine of sunflower particles is comprised of micro-spines with ~2−3 μm length (Table 1), and the spine-spine distances of ~2.9 μm. Based on similarity of the sizes and spacing of pollen spines and stigma papillae, one might expect alignment and optimization of their contact area under loading. In the subsequent AFM studies, to exclude the contributions of capillary forces contributed by liquids on the plant surfaces and focus on the surface morphology effects as mediated by VDW forces, we utilized cleaned sunflower pollen (Psf_C) and stigma, from which pollenkitt and surface secretions had been removed. Two relatively smooth and flat surfaces, silicon (Si, R_a = 0.2 nm) and PS (R_a = 2.2 nm) (Table 2), were utilized as control substrates for comparison with the stigma.

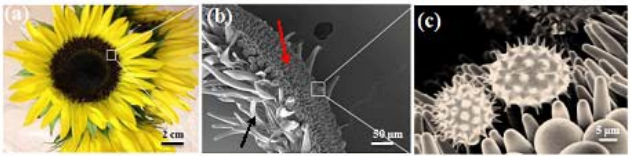

Figure 1. (a) Photograph of the sunflower (*Helianthus annuus*); (b) SEM image of one arm surface of sunflower stigma, showing the multi-rows of papillae (red arrow) and the long terminal hairs (black arrow); (c) SEM image of sunflower pollen on the stigma.

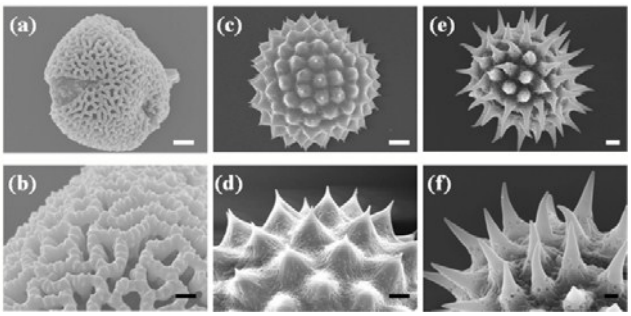

Figure 2. SEM images of clean pollen particles: (a) and (b) are olive pollen (Po_C); (c) and (d) are ragweed pollen (Pr_C); (e) and (f) are sunflower pollen (Psf_C). The white and black scale bar represent 2 μm and 500 nm, respectively.

Table 1. Characteristics of Pollen Particles.

Pollen	Morphology				Pollenkitt (mass%)
	Shape	Size (D, μm)	Height[a] (μm)	Radius[a] (nm)	
Olive	reticulate	20 ± 3	0.1─0.2	50 ± 5	8 ± 4
Ragweed	echinate	15 ± 3	0.5─1.0	52 ± 5	15 ± 5
Sunflower	echinate	30 ± 4	2.0─3.0	120 ± 10	30 ± 5

[a]Height and radius at tip of reticulate bumps or echinate spines.

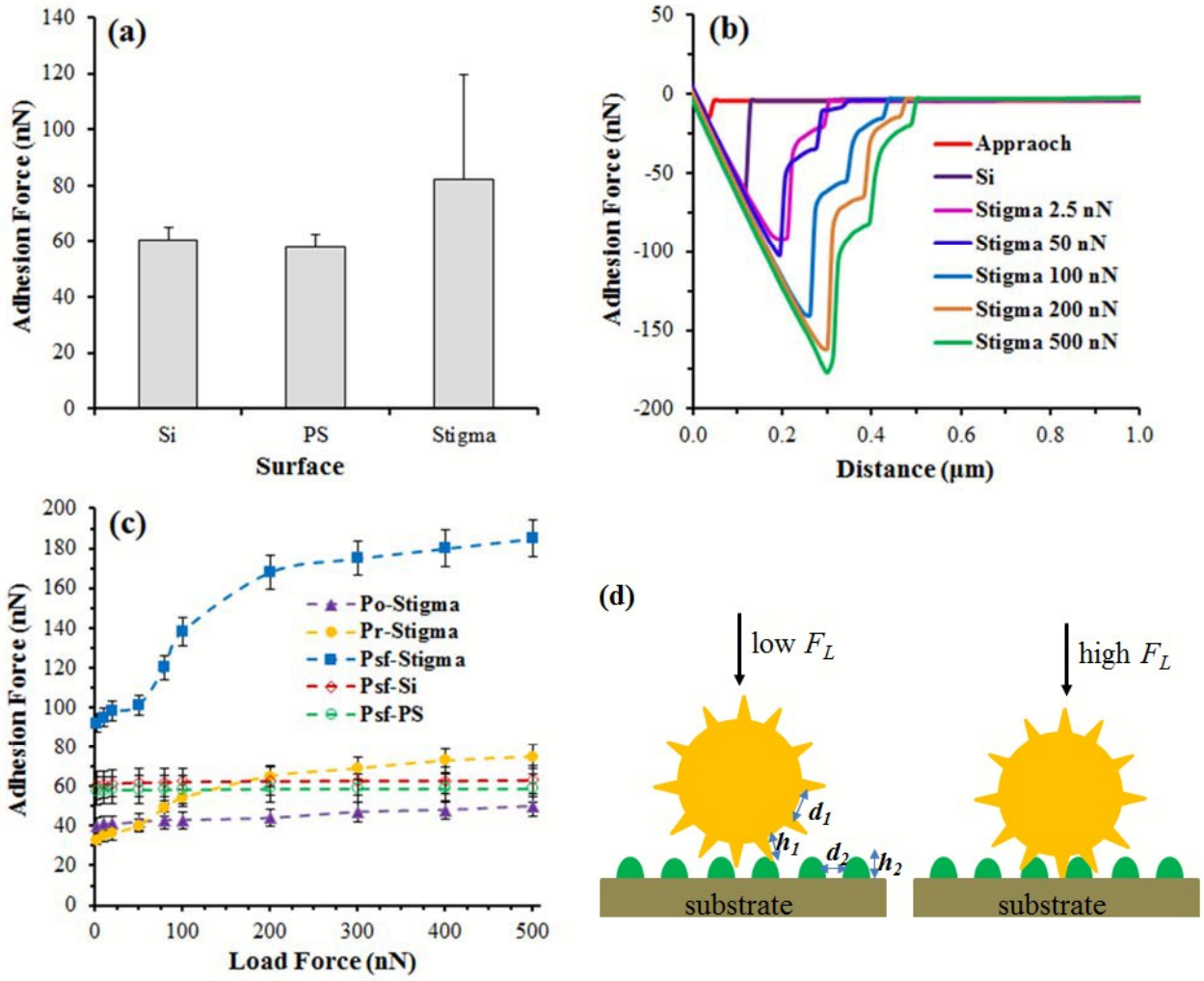

Figure 3. (a) Adhesion forces (F_{ad}) between the clean sunflower pollen (Psf_C) and three different substrates (Si, PS and Stigma) under 2.5 nN load force (F_L). (b) Typical adhesion force (F_{ad}) versus distance curves of clean sunflower pollen particles approach and retraction with Si and stigma surfaces as labelled. (c) F_{ad} versus F_L for each pollen particles interacting with three different substrates. Error bars are 95% confidence intervals. (d) 2D Schematic of interlocking interactions of echinate pollen spines with stigma-patterned surfaces under load forces.

As shown in Figure 3a, under a low load force of 2.5 nN, the AFM adhesion forces of clean sunflower pollen on Si and PS were ~60 nN with a small variation (95% confidence intervals <5 nN).[43, 51] In contrast, sunflower pollen particles exhibited a larger average adhesion force (~90 nN) with a much larger deviation (95% confidence intervals ~40 nN), corresponding to measurement variation on different locations on the clean stigma surface. These results suggest that only one spine of Psf_C particle contacts with smooth Si or PS surfaces, as observed in previous work,[43, 51] but the pollen-stigma contact is very dependent on the orientation of the pollen spines with the underlying papillae on the stigma. The number of pollen spines contact with stigma is varied from 1 to 6 (Figure 1c), which changes as the AFM pollen probe moves to different positions on the stigma. This hypothesis was confirmed by the typical force-distance curves shown in Figure 3b. As the AFM pollen probe approached the substrates, it experiences a jump to contact attraction attributed to the VDW attractive force (5 ± 3 nN). Upon retraction of the probe, the adhesive force increased linearly (indicated as movement towards negative forces in Figure 3b).

Table 2. Surface roughness of the various substrate surfaces (uncertainty is ± 95% confidence interval).

Film	Si	PS	PSI1	PSI2	PSI3
R_a (nm)	0.2 ± 0.1	2.2 ± 0.2	4.8 ± 0.8	10.4 ± 2.0	49.3 ± 6.0
R_{rms}(nm)	0.3 ± 0.1	2.7 ± 0.2	4.2 ± 0.9	14.3 ± 4.0	63.6 ± 8.0

Typically, one sudden pull-off separation (< 5 nm) of a Psf_C pollen particle was observed on smooth surfaces (Si and PS) for one spike contact.[43] However, two or more long-range pull-off separations (~100−300 nm) were observed during retraction of Psf_C particles from the stigma surface, which we attribute to the multiscale contact behaviors of pollen spines with the dense micro-patterned papillae of the stigma. The large variance of the overall adhesion forces on different areas of the stigma surface was attributed to the roughness and orientation/alignment of pollen particle and stigma papillae.

In order to verify whether the variation in adhesion forces are related to deformation of either pollen or stigma, the gradients of the force-distance data during contact in order to make comparisons of the representative the stiffness of the contact surfaces. As shown in Figure 3b, the gradient of the measured forces in the contact region for Si and stigma surfaces was calculated as 0.5 ± 0.1 N/m, which was comparable to the spring constant of the typical cantilever (~0.5 N/m). In contrast, for a control soft substrate, PDMS (Young's modulus 1−2 MPa), the gradient in the contact region was calculated as 0.08 ± 0.01 N/m (Figure S2), much lower than the spring constant of the cantilever. These results indicated that the pollen, Si and stigma surfaces are stiffer than the AFM cantilever, suggesting the force response is due to cantilever spring deflection and that there is no significant deformation of either pollen or substrate (Si and stigma). This is consistent with the absence of observable permanent deformations in SEM images in Figure S1.[54]

Interestingly, we observed a strong pressure-sensitive adhesion between echinate pollen particles (Pr_C and Psf_C) and stigma surfaces, as shown in Figure 3b and c. For example, under loading forces (F_L) up to 500 nN, the adhesion forces (F_{ad}) of Psf_C on Si and PS surfaces are almost constant (~60 nN) and independent of the load applied, suggesting no pressure effect and no substrate or pollen deformation. In marked contrast, a strong dependence on load F_L was observed for the pollen particles interacting with the stigma surface. The F_{ad} versus F_L curve showed three regimes: below F_L = 50 nN the adhesion forces increased slowly from ~90 nN to 100 nN; between F_L = 50 and 200 nN F_{ad} increased steeply; and above 200 nN no appreciable increase was observed and F_{ad} reached a plateau around 180 nN. It is instructive to compare this adhesion to the force required to detach a single Psf_C spine from a substrate surface, which can be estimated by the sphere-plane Hamaker model:[55]

$$F_{Hamaker} = \frac{AR}{6d^2} \quad (2)$$

where A is the material-dependent non-retarded Hamaker constant, R is radius of contact (estimated as the pollen spine radius, i.e., 120 ± 10 nm for sunflower pollen), and d is the cutoff separation distance, taken to be 0.165 nm. A was taken from the previous pollen adhesion measurements, as 8.5 × 10^{-20} J, which was invariant for the substrates used here.[43] According to Equation 2, the predicted adhesion force for a single spine tip of Psf_C in contact on a flat substrate, 61 ± 5 nN, was consistent with the previous experimental result.[55] Thus, an adhesion force of 90 nN suggests that more than one spine may be in contact with the stigma surface at low load. As loading increases, the increased pull-off adhesion suggests that either the surface area of contact and/or the number of spine contacts with the stigma was increasing with load forces beyond F_L of 50 nN. As indicated in Figure 1c, the pollen spines are roughly arranged at a spacing that is complementary to the size of the receptive papillae on the stigma. This complementarity can explain the observed loading-dependent adhesion, considering that the spines could align with the complementary-patterned surfaces of the papillae, resulting in increased contact area. Once the patterns have aligned, further loading would be unlikely to result in higher adhesion, which is consistent with the plateau at 180 nN. Figure 3d provides a 'drawn-to-scale' schematic of the alignment that is possible between the spines and the papillae, and measurements of the spine and papillae spacings indicate that they are in close agreement, e.g., $h_1 \approx h_2 \approx 2$ μm and $d_1 \approx d_2 \approx 2$ μm. An alternative explanation that should first be eliminated is that the pollen spines are simply indenting into the stigma surface and increasing contact area through deformation of the stigma surface. Several considerations cast doubt on this idea. First, as mentioned above, the stiffness of the cantilever-pollen-substrate system upon loading is nearly identical for both hard silicon substrates and the stigma surface under load forces up to 500 nN, as shown in Figure 3b. If significant indentation occurred, a lower gradient at the contact region would be observed upon loading the stigma. In addition, the sigmoidal shaped profile in Figure 3b, with a minimum loading force and a plateau, is not consistent with a continuously increasing elastic deformation. Careful examination of stigma surfaces after completion of adhesion measurements yields no evidence of permanent deformation indentations. On the other hand, the geometry of the sunflower pollen and stigma support the proposed pattern matching mechanism. This hypothesis was further conformed by replacing the echinate pollen particles with spherical reticulate olive pollen particle (Po_C) as the indenter. As shown in Figure 3c (dotted purple line), the adhesion force of Po_C on stigma surface is independent on the load forces, suggesting no permanent deformation indentations for spherical particles on stigma at pressure up to 500 nN.

This is the first known report of pattern-mediated pressure-dependent adhesion of pollen on stigma. It could provide important insights into the mechanism by which pollens that are already well adhered to a pollinator can be transferred onto a stigma. The estimated mass of a typical pollinator, a honey bee, is ~20 mg, a mass that could provide a loading force of 200 μN, which is above the threshold of 50 nN required to observe the loading-force dependent adhesion in Figure 3b. The resulting 180 nN adhesion force is strong enough to resist the drag forces created by an air velocity up to 3 m/s. Beyond the importance in the natural system, we believe that this is the first report of a microparticle exhibiting a pressure-sensitive adhesion that is mediated by physical patterns that interlock with a substrate. This new concept could provide inspiration for novel adhesion and transport designs in applications involving soft matter. If the adhesion is driven by pattern matching between pollen and stigma, as claimed, then it should be sensitive to physical parameters like the length, tip radius and spacing of both spines and papillae. To test the hypothesis, as well as to demonstrate that these features can be mimicked, we fabricated polymeric patterned surfaces with surface features that have tunable size and spacing.

Fabrication of Stigma Mimicking Patterned Polymer Surfaces

Blends of PSI copolymer with PS homopolymer with appropriately-chosen M_w result in a controllable phase separation that produces a repeatable pattern that mimics features of the stigma surfaces. Below, we held the PS:PSI mass ratio at 1:4 while varying just the PS M_w. In Figure 4, AFM images indicate the distinct rough structures of the blended polymer films PSI1, PSI2, and PSI3. The R_a values were 4.8 nm, 10.4 nm, and 49.3 nm for PSI1, PSI2, and PSI3, respectively, indicating that an order of magnitude range of control in roughness can be achieved by adjusting the PS M_w. The height of the most prominent features, which appear to be PS protruding from the surface based on arguments presented below, increased dramatically upon increasing the PS M_w: the height of PS

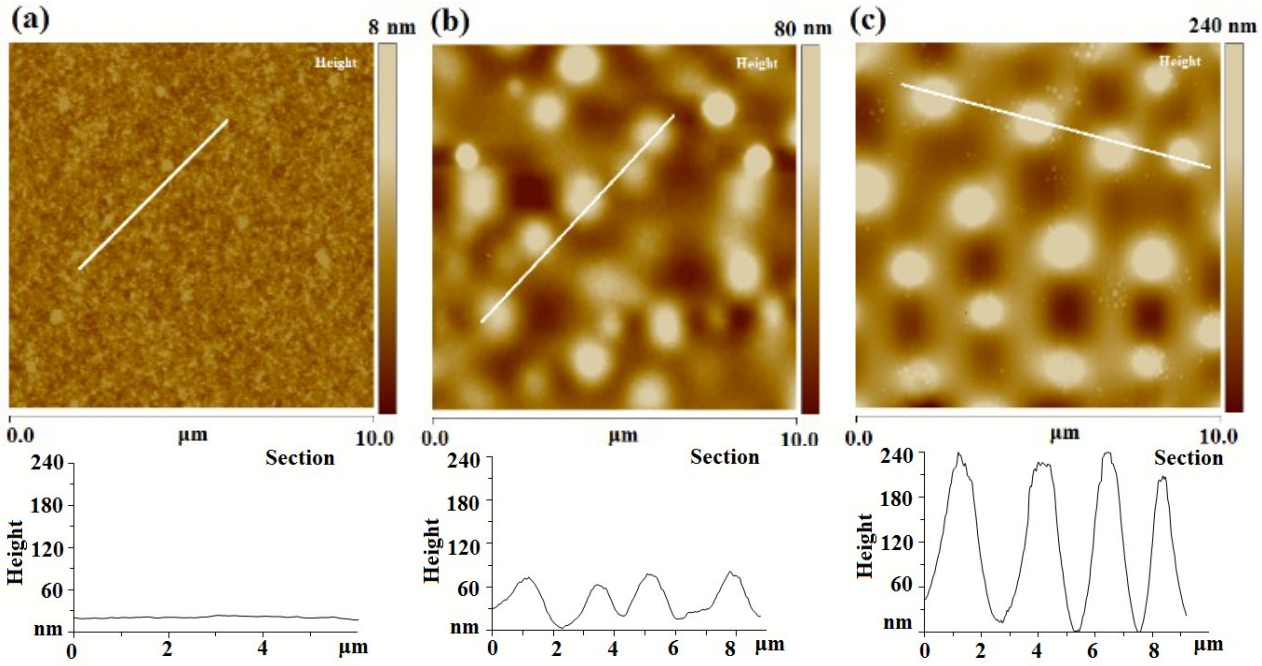

Figure 4. AFM contact mode images of conical-patterned polymer surfaces (10 µm×10 µm). The films were assembled from (a) PSI1, (b) PSI2, and (c) PSI3.

domains increased from 4−8 nm (PSI1) to 210−240 nm (PSI3). Further, the peak to peak distances for the PS domains of PSI2 andPSI3 are 1.7 ± 0.9 µm for PSI2 and 2.5 ± 0.6 µm for PSI3, which are close to the inter-papillary (4 ± 2 µm) spacing on the sunflower stigma and are also close to the spine-spine distances of ~2.2 µm and ~2.9 µm for ragweed and sunflower pollens (Figure 2), respectively. Hence, the range of surface features presented here are in an acceptable range for providing controls to test the pattern sensitivity of echinate pollen adhesion.

While asymmetric ABA triblock copolymers with short A blocks and sufficient total molecular mass are known to form a cylindrical microphase-separated structure with A within the cylinders,[56, 57] block copolymer ordering is not driving the structures observed in Figure 4. Rather, macroscopic phase behavior between PS and PSI governs the observed structures. Because the M_n of PSI is low, 1300 Da, and there are ~2 styrene monomers on each end at 13 wt.%, it is doubtful that this triblock forms an ordered microphase-separated state, because χN is expected to be < 10.[56] In addition, even if the PSI formed an ordered microphase, the homopolymer A can be dissolved in the corresponding microdomain of ABA only if the homopolymer molecular mass $M_{A,H}$ is less than or not too far above that of the A block in the block copolymer, $M_{A,ABA}$.[57, 58] This condition is not met for any of the homopolymers utilized in our study, since $M_{A,ABA}$ ~ 160 Da (roughly 2 styrene monomers), and $M_{A,H}$ is either 1,900 Da (PS1), 13,000 Da (PS2) or 230,000 Da (PS3). When $M_{A,H}>M_{A,ABA}$, the homopolymer is expected to forms a second phase separate from the copolymer (for $M_{A,H} >> M_{A,ABA}$).[57, 58] Because of low total molecular masses we expect the PSI/PS1 blend to be miscible, and the relatively small 4−5 nm roughness with lack of discernable ordering observed in Figure 4 is consistent with this expectation. The relatively low T_g values of PSI (T_g = -40 °C) and PS1 (T_g ~ 34 °C) also support liquid-like mobility at the annealing T of 80 °C, and therefore good mixing if the low M_n components are compatible. On the other hand, when the PSI is blended with higher M_n PS2 and PS3, macrophase separation between PS and PSI is expected during the drying process.[57, 58] Furthermore, the T_g of PS2 (90 °C) and PS3 (104 °C) are higher than the annealing temperature, indicating they approach a glassy condition as solvent is removed. Thus, the phase-separating PS drops are expected to behave as a dispersed colloidal phase within the rubbery PSI. Figure 4 reveals that raised structures with nearly hexagonal ordering on the length scale of a few particle diameters are observed for PSI2 and PSI3. In fact, optical microscope images indicate that phase segregated hard domains of PS form lens-like protrusions through the PSI film surface (not shown). We reason that the micrometer-range ordering among the PS spheres within the PSI matrix arises from attractive depletion forces between the PS colloid induced by the short, non-adsorbing PSI copolymer during solvent drying.[59] It is reasonable to expect that PSI does not adsorb on the high M_w PS drops because the ~2 monomers of styrene on the ends of PSI are unlikely to overcome the incompatibility between styrene and isoprene and the loss in entropy associated with forming a poly(isoprene) loop at the surface. Similar mixtures of short chain polymers with large colloidal particles are known to produce depletion-induced colloidal crystalline phases even at low particle volume fractions, especially as the overlap concentration is approached for the polymer, which we expect during drying. [59]

Tuning of Pressure-Sensitive Particle Adhesion to Stigma-Mimicking Surfaces

The design and fabrication of functional patterned polymer surfaces, where chemical or charge complementarity is used for tuning enhanced, selective and controllable adhesion, have captured widespread scientific interest in recent years.[30-32, 60-62] Here, the

adhesion forces of pollen particles onto stigma-mimicking patterned surfaces can be tuned by the patterned surface roughness, pollen micro-structures and load forces. Figure 5a shows the adhesion forces of three different clean pollen particles of each species (Po_C, Pr_C and Psf_C) with each stigma-mimicking patterned substrate measured by AFM method under a low load (2.5 nN). Olive was chosen, along with ragweed and sunflower, to test the sensitivity of pressure-dependent adhesion to the presence or absence of spine structures on the pollen. Figure 5b shows typical force-distance curves for a clean sunflower pollen particle interacting with PSI1, PSI2 and PSI3 patterned surfaces. On the smoothest surfaces (R_a < 5 nm, i.e., Si, PS and PSI1), we always observed the attachment and detachment of only one pollen spine or contact point for all the particles of three pollen species. In contrast, for substrates with surface roughness of R_a > 10 nm (PSI2 and PSI3), pollen particles display multiple contacts (up to three spikes) and larger adhesion forces for ragweed and sunflower particles, as shown in the force-distance curves in Figure 5b. Multiple contacts are indicated by arrows in the force distance curves. Furthermore, only 50 % of AFM force measurements of sunflower pollen with the PSI2 surface showed two spines contacting; however, for the PSI3 surface, more than 90% of measurements showed two or three spines contacting simultaneously. The details of the related force-distributions of each pollen species interacting with those three stigma-mimicking patterned substrates (PSI1, PSI2 and PSI3) were shown in Figure S4. The multiple contacts, together with knowledge that the spine and substrate patterns are similar in size (as shown in Figures 2 and 4), suggest that an interlocking arrangement that optimizes contact area may cause enhanced adhesion as inspired by the interactions of pollen-stigma shown above. In order to verify and exclude the effect of the surface chemistry on the pollen adhesion on those surfaces, control experiments of pollen adhesion on all three PS (PS, PS1 and PS2) and PSI surfaces were also conducted. As shown in Figure S5, we didn't observe significant changes of the adhesion forces for each pollen on all those surfaces. Further, under the same series of load forces (up to 500 nN), those adhesion forces were also not changed.

Interestingly, increased load forces should be able to force the alignment of pollen spines with surface features on PSI2 and PSI3, which would show up as increased adhesion on these surfaces. In contrast, adhesion should be loading independent for olive (reticulate) pollen on all surfaces as well as for echinate (ragweed, sunflower) on the smoothest surfaces. As shown in Figure 6 and S6a, with increasing load forces, the adhesion forces of clean sunflower pollen particles interacting with the two roughest and better pollen-spiked matched ($d_1 \approx d_2$) surfaces, PSI2 and PSI3, increased proportionately from ~90 nN to ~160 nN between 2.5 nN and 500 nN load forces. The ragweed adhesion force increased proportionately also on PSI2 and PSI3. However, the adhesion force of clean olive particles with reticulated surface interacting with PSI2 and PSI3 was not significantly changed with the load forces. The load dependence suggests the forced alignment of pollen spikes with the pattern on the rough patterned polymer surface under higher loads. In contrast, as Figure 6 shows for PSI1, Si, and PS, the adhesion forces for all the pollen species in contact with the three smoothest surfaces were independent of load forces. In Table S1 we provide *p*-values for analysis of variance (ANOVA) between the different groups of substrates, used to reject / accept the hypothesis that these means are from the same groups (the null hypothesis). The results show that under the loading extremes, the only comparisons that have $p > 0.05$ (null accepted) are those for which we expect similarity, e.g., the two smoothest surfaces (PS and PSI1) and the two roughest surfaces (PSI2 and PSI3), for all three pollens at both the lowest (2.5 nN) and the highest (500 nN) loading. All other comparisons of substrates, for all three pollens and two loading extremes, have independent means (null rejected), with very low p values, e.g., $p < 0.0055$.

Some sources of load-dependent behavior should be considered in addition to pattern interlocking. One could argue that the pollen spines on ragweed or sunflower imbed in the softer PSI phase, and that this imbedding behavior produces increased surface area that results in the increasing adhesion. However, we do not believe this is a significant effect because it would be expected to result in a non-linear increase in adhesion (as multiple 'cone'-shaped spines are pushed deeper into the surface). More importantly, load-dependent behavior is not observed for ragweed or sunflower on the PSI1 surface, which is composed of 75 wt% PSI and the remainder low M_n PS oligomer, is expected to be as soft as the PSI phase in PS2 and PS3. Furthermore, the gradients at the contact region of force-distance curves (Figure S3a) for the Psf_C probe on PSI3 surfaces are identical for the load forces up to 500 nN, suggesting no deformations of their contact interactions as mentioned above. In conclusion, during the AFM adhesion force measurements, the pollen particles displayed two or three spines in contact with patterned rough polymer surfaces, but adhesion magnitude was highly variable. Adhesive forces were dependent on load force for the roughest stigma-mimicking-patterned matched polymer surfaces (PSI2 and PSI3) interacting with the most pronounced ornamentations (ragweed and sunflower). We believe this is due to the limited orientations offered by the pollen particles immobilized in a fixed position on the cantilever.

Two alternative explanations (other than interlocking patterns) to the load dependent behavior can be considered. First the difference in chemical identity of the poly(styrene) and poly(isoprene) phases might contribute to increased adhesion on PSI2 and PSI3. However, control experiments on the individual polymer components PS, PI1, PI2, and PI3 indicate essentially identical van der Waals adhesion on all of these substrates (Figure S5). Secondly, one should consider whether buckling of the cone-like pollen spines could explain the loading dependence observed for ragweed and sunflower pollens. Control experiments of adhesion force measurements of pollen particles with flat surfaces (i.e. Si and PS in Figures 6) show no significant force changes indicative of buckling with increasing load. In SEM images of pollen spines taken after AFM measurements, including those in Figure 2, we have not observed evidence of buckled spines. Analytical expressions for the critical load to buckle a truncated cone have been derived, but require an elastic modulus value. An estimate of the ragweed sporopollenin compressive modulus of ~1.6 GPa can be taken from Liu et al.[63] Using this modulus, one can calculate the critical load to buckle a truncated cone with base radius R_1 = 1000 nm, end radius R_2 = 100 nm, and length L = 4000 nm (similar to sunflower pollen) to be P_c = 9900 nN.[64] All of the loads fall well under this value, and taking into consideration the absence of microscopy evidence, we exclude buckling.

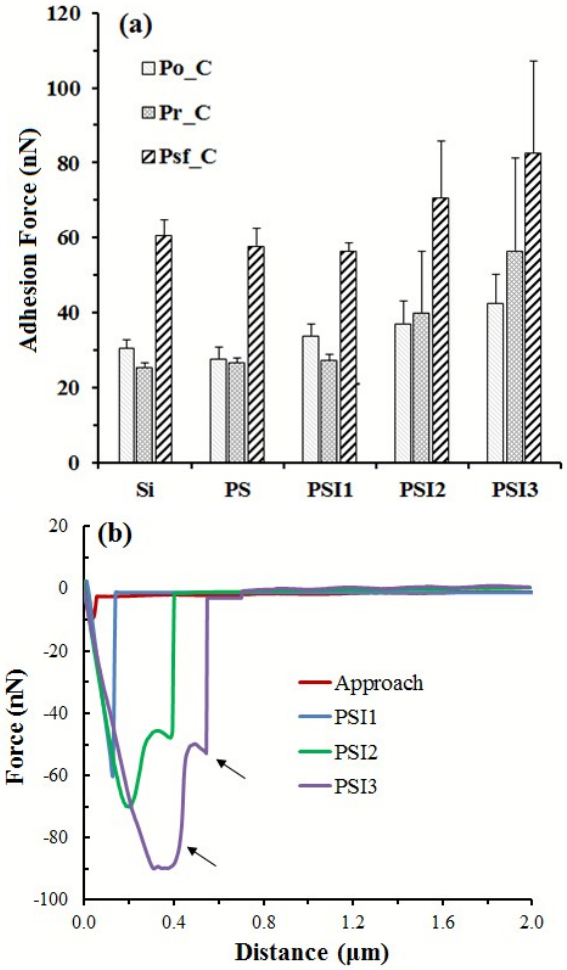

Figure 5. (a) Adhesion forces for three clean pollen particles of each species (Po_C, Pr_C and Psf_C) interacting with five different substrate surfaces (Si, PS, PSI1, PSI2 and PSI3) under load force 2.5 nN. Error bars are 95% confidence intervals. (b) Typical force-distance curves of a clean sunflower pollen particle (Psf_C) interacting with PSI1, PSI2 and PSI3 surfaces as labelled. Arrows indicate at least two spines contact the surfaces.

For native pollen particles with liquid pollenkitt intact, as shown in Figure S6b and S7, the adhesion force magnitudes were dramatically increased relative to clean particles, for example from 60 nN for clean Psf to 145 nN for native Psf. As reported previously, the adhesion-enhancing effect of pollenkitt is driven by the formation of pollenkitt capillary bridges and was species-dependent, with echinate insect-pollinated species (sunflower) showing significantly stronger adhesion and higher substrate dependence than wind pollinated species (ragweed and olive).[43] This species-dependent pollenkitt effect is due to the combination of high pollenkitt volume (~30 wt.% pollenkitt in Psf_N) and large convex/spiny surface features in echinate *entomophilous* varieties, improving the spreading area of the liquid pollenkitt relative to varieties of pollen with less pollenkitt volume (~8 wt.% and 15 wt.% pollenkitt in Po_N and Pr_N, respectively) and smaller ornamentations. Interestingly, we observed that pollenkitt increases the magnitude of pressure-sensitive adhesion to stigma-mimicking-patterned surfaces, relative to clean pollens, as shown in Figure S6b and S7. For native ragweed and sunflower particles, the adhesion forces were increased by up to 4 times with the load forces increasing from 2.5 to 500 nN, while the increase for clean particles was only about 1.5−2 times under the same conditions. These results suggest that the liquid pollenkitt film on the pollen shell may lubricate the interfaces and support spine interlocking with the patterned surfaces, as confirmed by the force-distances curves in Figure S6.

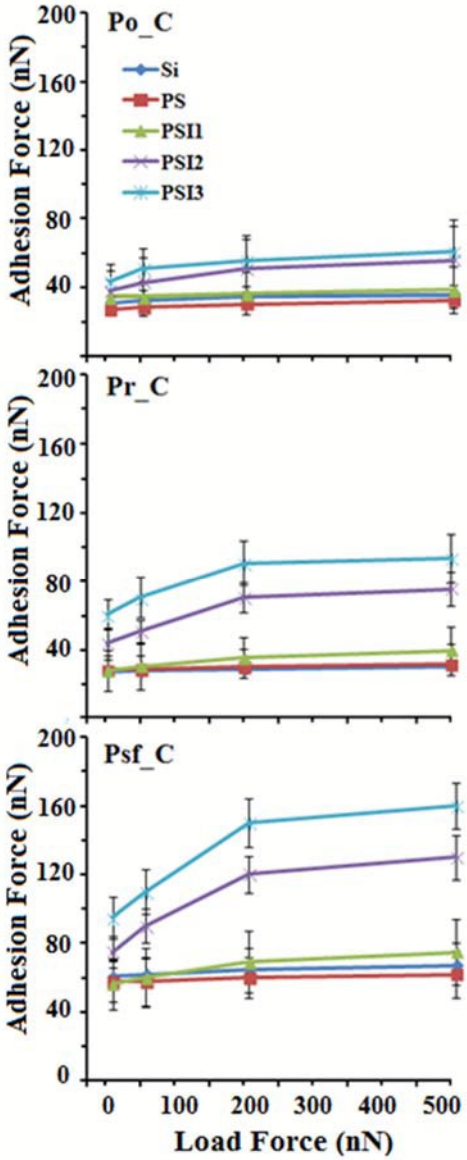

Figure 6. Adhesion forces versus load forces for clean pollen particles of each species interacting with five different substrate surfaces. Error bars are 95% confidence intervals.

Detachment Force from Surfaces

Another important characteristic of the interaction of particles on surfaces is the particle detachment behavior, which was measured by a centrifuge method. An advantage of this technique relative to AFM is that the freely-orienting pollens that deposit on the substrate allow

sampling of a larger population of orientations and particles. Plots of retained percentage of adherent particles versus the centrifugal force are shown in Figure 7. The detachment force (F_d) was defined as the centrifugal force at 50% retained percentage, and the values are listed in Table 3 for all three clean and native pollen species from four substrates with varied surface roughness (PS, PSI1, PSI2 and PSI3). For each pollen species, the F_d increased with surface roughness, suggesting more contact area between particles with rougher surfaces. However, the percent retained increased dramatically for sunflower grains on the PSI2 and PSI3 surfaces (with 10 nm and 49 nm R_a, respectively), compared to the PS and PSI1 surfaces (with 2 nm and 5 nm R_a, respectively). The F_d magnitude of sunflower particles and its percentage increase on the 10 nm and 49 nm surfaces was far above the range observed for other pollens. In fact, the F_d of native sunflower pollen particles on these two roughest surfaces was much larger (>1600 nN) than that of ragweed (800 ± 60nN) and olive (760± 50nN). For most of the force range sampled by the centrifuge, the percent retained jumps to values near 95% for Psf on PS2 and PS3, in stark contrast the behavior of Psf on the smoother surfaces, and to the behavior of Po and Pr on any surface. This behavior is consistent with the evidence of an interlocking configuration of the spines and the substrate observed by AFM measurements on the synthetic PSI2 and PSI3 surfaces, as well as the same behavior observed between Psf and native stigma surfaces

Table 3. The detachment forces obtained from centrifuge method for clean and native pollen particles on various polymer substrates.

F_d (nN)	Surface			
	PS	PSI1	PSI2	PSI23
Po_C	180 ± 44	200 ± 60	240 ± 40	300 ± 40
Pr_C	140 ± 45	160 ± 40	360 ± 60	400 ± 80
Psf_C	400 ± 60	480 ± 95	860 ± 80	1120 ± 80
Po_N	380 ± 40	500 ± 50	760 ± 50	1000 ± 60
Pr_N	360 ± 45	480 ± 50	800 ± 60	960 ± 96
Psf_N	880 ± 65	1150 ± 80	>1600	>1600

The F_d values are in some cases considerably higher than the pull-off forces measured by AFM (see supplementary Figure S7 for AFM adhesion forces of native pollenkitt-coated pollens). It is important to remember that the AFM results represent a few particle orientations only, and also they represent direct pull-off normal to the substrate. The centrifuge results, on the other hand, represent many hundreds of particles and sample a larger range of orientations. As mentioned above, due to the limitation of tip orientation in the AFM method, we only observe one spine interacting with smooth surfaces and two or three spines sometimes contacting with the rougher surfaces using the AFM technique. However, when the spiked pollen is deposited freely on surfaces, one observes more contacts, in some cases 5−6 contacts on a flat surface, as indicated in Supplementary Figure S8.

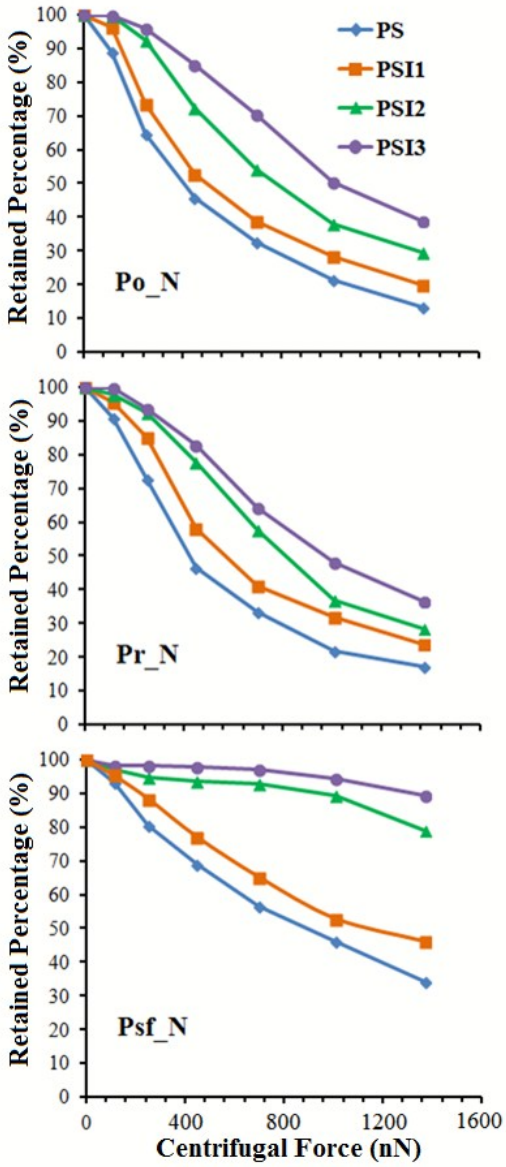

Figure 7. Detachment profiles by retained percentage (%) versus centrifugal force (nN) for native pollen on substrates with various roughness values.

Conclusions

Here, we report the first observation of pattern-mediated pressure-sensitive adhesion of a microparticle, by observing the adhesive forces of sunflower pollens on native sunflower stigma surfaces. Evidence suggests that the strong pressure-sensitive adhesion arises from the interlocking of complementary-sized patterns of the pollen spines and stigma surfaces. Inspired by the stigma surface, a series of tunably-patterned polymer surfaces were fabricated by the phase-separation of blends of PS with PSI, which enabled mimicry of the pressure-sensitive adhesion. A result of the mimicked surfaces was that the pattern and pressure sensitive adhesion is active only for echinate (spiny) pollens and only for surfaces with features with average roughness of at least 10 nm. We also found that including

the liquid pollenkitt coating on the pollen serves to amplify the pattern- and pressure-sensitive effects, through the combination of interlocking solid-solid adhesion with capillary forces. This work indicates that pollens and stigma surfaces could serve as a new model system for biomimicry-based design of adhesion on a micro-particle size scale and on force scales in the 10 to 1000 nN range. These are likely to be useful in advanced soft materials applications including paints, coatings, drug delivery, and composites, among others.

Acknowledgements

Acknowledgment is made to AFOSR grant number FA955010-1-0555 for financial support.

Appendix A. Supplementary material

The supporting information available on-line provides SEM images of pollen probes, a typical force-distance curve for the interactions of Psf_C and a flat PDMS substrate, force-distance curves for the interactions of sunflower pollen AFM probes and PSI3 substrate at a serious of load forces, figures of adhesion forces for the interaction of native pollenkitt-coated pollen particles with five different substrate surfaces at a serious of loading forces, and figures of SEM images of pollen multiple spines contact to surfaces.

Corresponding Author

J. Carson Meredith, Email: carson.meredith@chbe.gatech.edu

References

1. J. Park, Y. Lee, J. Hong, M. Ha, Y. Jung, H. Lim, S. Y. Kim and H. Ko, *Acs Nano*, 2014, **8**, 12020-12029.
2. L. F. Boesel, C. Greiner, E. Arzt and A. del Campo, *Advanced Materials*, 2010, **22**, 2125-2137.
3. H. E. Jeong, J.-K. Lee, H. N. Kim, S. H. Moon and K. Y. Suh, *Proceedings of the National Academy of Sciences of the United States of America*, 2009, **106**, 5639-5644.
4. F. Xia and L. Jiang, *Advanced Materials*, 2008, **20**, 2842-2858.
5. D.-H. Kim, N. Lu, R. Ma, Y.-S. Kim, R.-H. Kim, S. Wang, J. Wu, S. M. Won, H. Tao, A. Islam, K. J. Yu, T.-i. Kim, R. Chowdhury, M. Ying, L. Xu, M. Li, H.-J. Chung, H. Keum, M. McCormick, P. Liu, Y.-W. Zhang, F. G. Omenetto, Y. Huang, T. Coleman and J. A. Rogers, *Science*, 2011, **333**, 838-843.
6. T.-i. Kim, H. E. Jeong, K. Y. Suh and H. H. Lee, *Advanced Materials*, 2009, **21**, 2276-+.
7. L. P. Lee and R. Szema, *Science*, 2005, **310**, 1148-1150.
8. C. Pang, S. M. Kim, Y. Rahmawan and K.-Y. Suh, *Acs Applied Materials & Interfaces*, 2012, **4**, 4225-4230.
9. S. N. Gorb, *Proceedings of the Royal Society B-Biological Sciences*, 1999, **266**, 525-535.
10. M. Scherge and S. Gorb, *Biological Micro-And Nanotribology: Nature's Solutions*, Springer, 2001.
11. Y. Li, J. H. Zhou, C. Zhang, C. Menon and B. D. Gates, *ACS Appl Mater Interfaces*, 2015, **7**, 2340-2348.
12. M. Sitti and R. S. Fearing, *Journal of Adhesion Science and Technology*, 2003, **17**, 1055-1073.
13. Y. Zheng, H. Bai, Z. Huang, X. Tian, F.-Q. Nie, Y. Zhao, J. Zhai and L. Jiang, *Nature*, 2010, **463**, 640-643.
14. J. Yu, S. Chary, S. Das, J. Tamelier, K. L. Turner and J. N. Israelachvili, *Langmuir*, 2012, **28**, 11527-11534.
15. J. Sun and B. Bhushan, *Rsc Advances*, 2012, **2**, 12606-12623.
16. E. Arzt, S. Gorb and R. Spolenak, *Proceedings of the National Academy of Sciences of the United States of America*, 2003, **100**, 10603-10606.
17. C.-M. Chen, C.-L. Chiang, C.-L. Lai, T. Xie and S. Yang, *Advanced Functional Materials*, 2013, **23**, 3813-3823.
18. C. Pang, G.-Y. Lee, T.-i. Kim, S. M. Kim, H. N. Kim, S.-H. Ahn and K.-Y. Suh, *Nature Materials*, 2012, **11**, 795-801.
19. M. M. Gotelli, B. G. Galati and D. Medan, *Biocell*, 2010, **34**, 133-138.
20. R. B. Knox, *J Cell Sci*, 1973, **12**, 421-443.
21. H. Wu, M. Li and M. Sun, *Chinese Science Bulletin*, 2008, **53**, 1015-1020.
22. G. M. Zinkl, B. I. Zwiebel, D. G. Grier and D. Preuss, *Development*, 1999, **126**, 5431-5440.
23. A. F. Edlund, R. Swanson and D. Preuss, *Plant Cell*, 2004, **16**, S84-S97.
24. P. Heizmann, D. T. Luu and C. Dumas, *Annals of Botany*, 2000, **85**, 23-27.
25. D. T. Luu, P. Heizmann and C. Dumas, *Plant Physiology*, 1997, **115**, 1221-1230.
26. D. T. Luu, D. Marty-Mazars, M. Trick, C. Dumas and P. Heizmann, *Plant Cell*, 1999, **11**, 251-262.
27. G. D. Mestral, *Patents US3009235 A*, 1961.
28. M. Lamblet, E. Verneuil, T. Vilmin, A. Buguin, P. Silberzan and L. Leger, *Langmuir*, 2007, **23**, 6966-6974.
29. H. Shahsavan and B. Zhao, *Langmuir*, 2011, **27**, 7732-7742.
30. S. Vajpayee, K. Khare, S. Yang, C.-Y. Hui and A. Jagota, *Advanced Functional Materials*, 2011, **21**, 547-555.
31. A. K. Singh, Y. Bai, N. Nadermann, A. Jagota and C.-Y. Hui, *Langmuir*, 2012, **28**, 4213-4222.
32. C. Jin, A. Jagota and C.-Y. Hui, *Advanced Functional Materials*, 2013, **23**, 3453-3462.
33. M. Lorch, M. J. Thomasson, A. Diego-Taboada, S. Barrier, S. L. Atkin, G. Mackenzie and S. J. Archibald, *Chem Commun (Camb)*, 2009, DOI: 10.1039/b909551a, 6442-6444.
34. M. S. Hassan and R. Lau, in *13th International Conference on Biomedical Engineering, Vols 1-3*, eds. C. T. Lim and J. C. H. Goh, 2009, vol. 23, pp. 1434-1437.
35. S. Barrier, A. Diego-Taboada, M. J. Thomasson, L. Madden, J. C. Pointon, J. D. Wadhawan, S. T. Beckett, S. L. Atkin and G. Mackenzie, *Journal of Materials Chemistry*, 2011, **21**, 975-981.
36. A. Diego-Taboada, S. T. Beckett, S. L. Atkin and G. Mackenzie, *Pharmaceutics*, 2014, **6**, 80-96.
37. T. F. Tadros, *Colloids in Paints: Colloids and Interface Science*, WILEY-VCH, 2010.
38. J. H. Lee, B. M. Suttle, H. J. Kim and J. C. Meredith, *Macromolecular Materials and Engineering*, 2011, **296**, 1055-1062.
39. W. B. Goodwin, I. J. Gomez, Y. Fang, J. C. Meredith and K. H. Sandhage, *Chemistry of Materials*, 2013, **25**, 4529-4536.
40. I. J. Gomez, W. B. Goodwin, D. Sabo, Z. J. Zhang, K. H. Sandhage and J. C. Meredith, *Journal of Materials Chemistry C*, 2015, **3**, 632-643.
41. E. Pacini and M. Hesse, *Flora*, 2005, **200**.
42. E. Pacini, *Canadian Journal of Botany-Revue Canadienne De Botanique*, 1997, **75**, 1448-1459.
43. H. Lin, I. Gomez and J. C. Meredith, *Langmuir*, 2013, **29**, 3012-3023.
44. H. E. M. Dobson, *American Journal of Botany*, 1988, **75**, 170-182.
45. B. J. R. Thio, J. H. Lee and J. C. Meredith, *Environmental Science & Technology*, 2009, **43**, 4308-4313.

46. P. M. Toporowski and J. E. L. Roovers, *Journal of Polymer Science Part a-Polymer Chemistry*, 1976, **14**, 2233-2242.
47. L.-P. Blanchard, J. Hesse and S. L. Malhotr, *Canadian Journal of Chemistry*, 1974, **52**, 3170-3175.
48. D. K. Donald, *Journal of Applied Physics*, 1969, **40**, 3013-&.
49. D. F. Stjohn and Montgome.Dj, *Journal of Applied Physics*, 1971, **42**, 663-&.
50. W. F. Sheridan, *Maize for Biological Research*, Plant Molecular Biology Association, Charlottesville, 1982.
51. H. Lin, L. Lizarraga, L. A. Bottomley and J. Carson Meredith, *J Colloid Interface Sci*, 2015, **442**, 133-139.
52. A. H. Ibrahim, P. F. Dunn and R. M. Brach, *Journal of Aerosol Science*, 2003, **34**, 765-782.
53. T. T. Nguyen, C. Rambanapasi, A. H. de Boer, H. W. Frijlink, P. M. V. D. Ven, J. de Vries, H. J. Busscher and K. V. D. V. Maarschalk, *International Journal of Pharmaceutics*, 2010, **393**, 88-95.
54. S. Allen, M. C. Davies, C. J. Roberts, S. J. B. Tendler and P. M. Williams, *Trends in Biotechnology*, 1997, **15**, 101-105.
55. J. Israelachvili, *Intermolecular and Surface Forces*, Acadamic Press, London, 1992.
56. V. Abetz and P. F. W. Simon, *Advances in Polymer Science*, 2005, **189**, 125–212.
57. A. S. Krishnan, S. D. Smith and R. J. Spontak, *Macromolecules*, 2012, **45**, 6056-6067.
58. T. A. Mykhaylyk, O. O. Mykhaylyk, S. Collins and I. W. Hamley, *Macromolecules*, 2004, **37**, 3369-3377.
59. R. Tuinier, J. Rieger and C. G. d. Kruif, *Advances in Colloid and Interface Science*, 2003, **103**, 1-31.
60. J. T. Koberstein, *Journal of Polymer Science Part B-Polymer Physics*, 2004, **42**, 2942-2956.
61. E. Kokkoli and C. F. Zukoski, *Langmuir*, 2001, **17**, 369-376.
62. Y. Bai, C. Jin, A. Jagota and C. Y. Hui, *Journal of Applied Physics*, 2011, **110**.
63. T. Liu and Z. Zhang, *Biotechnol Bioeng*, 2004, **85**, 770-775.
64. W. G. Smith, *Computers & Structures*, 1988, **28**, 677-681.

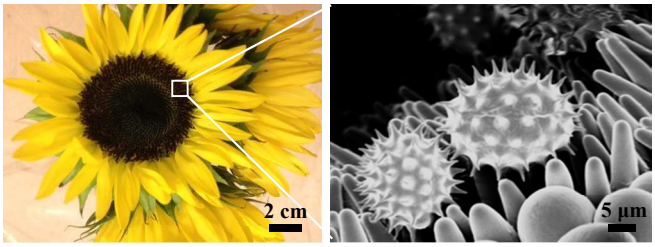

Biomimicry of structurally-derived pollen-stigma interactions enables pressure-sensitive microparticle adhesion.